Spectroscopic ellipsometry study of the diluted magnetic semiconductor system Zn(Mn,Fe,Co)Se

Y. D. Kim, S. L. Cooper, and M. V. Klein
Department of Physics and Materials Research Laboratory, University of Illinois at Urbana-Champaign, 1110 West Green Street, Urbana, Illinois 61801

B. T. Jonker
Naval Research Laboratory, 4555 Overlook Avenue, Southwest, Washington, D.C. 20375-5000
(Received 12 May 1993)

Single-crystal films of (001)$Zn_{1-x}A_xSe$ (A=Mn, Fe, Co) ($0 \le x < 0.14$) grown by molecular-beam epitaxy on (001)GaAs have been studied by spectroscopic ellipsometry in the 3.5–5.5 eV photon-energy range. Using fits of the E_1 and $E_1+\Delta_1$ peaks with a standard analytic expression, we find that the linewidths increase with x for all samples, the energies increase with x for $Zn_{1-x}Fe_xSe$ and $Zn_{1-x}Co_xSe$, and the energies decrease with x for $Zn_{1-x}Mn_xSe$. A model describing the effects of the *sp-d* exchange interaction on the L point band-gap energy is developed and applied. We find that the strength of the energy correction due to this interaction, which is proportional to the product of the square of the exchange integrals and the magnetic susceptibility of the material, is largest in Mn-doped and smallest in Co-doped ZnSe. While the *sp-d* exchange interaction model is consistent with the composition dependence of the E_1 and $E_1+\Delta_1$ band-gap energies in $Zn_{1-x}Mn_xSe$, it does not describe the behavior observed in $Zn_{1-x}Fe_xSe$ and $Zn_{1-x}Co_xSe$. We show that an *sp-d* hybridization model, which includes the location of the energy levels of the magnetic impurity *d* levels, can account for the composition dependence of E_1 and $E_1+\Delta_1$ band-gap energies of all three materials.

I. INTRODUCTION

Diluted magnetic semiconductors[1,2] (DMS's) are a class of semiconducting materials formed by randomly replacing some fraction of the cation in a compound semiconductor with a magnetic ion, e.g., Mn^{2+} in ZnSe ($Zn_{1-x}Mn_xSe$). The presence of the magnetic ion leads to a number of unusual electronic and optical properties, including a magnetically tunable band gap, resulting from the large *sp-d* exchange interaction between the magnetic ions and the band electrons.[3–9] This tunability has permitted the realization of spin polarized hole separation and a field tunable type-I/type-II band alignment,[10,11] as well as the formation of a true spin superlattice.[12–14] These interactions are strongly influenced by the ground state of the particular substitutional magnetic ion used. The Mn-based DMS family, in which the Mn^{2+} ($3d^5$) ion has a $^6S_{5/2}$ free-ion ground level, has been extensively studied, and their magnetic properties are fairly well understood.[2,5,6,14–19]

More recently, attention has been focused on Fe-based DMS materials,[20–27] whose properties are very different from their Mn-based counterparts. This is largely due to the more complicated level splitting of the Fe^{2+} ($3d^6$) ion,[28] which involves a ^5E ground state manifold that is split by the spin-orbit interaction into five closely spaced ($\sim$2.2 meV) levels. The ground state of this manifold is a nondegenerate A_1 ground state having no permanent magnetic moment. This configuration leads to Van Vleck paramagnetic behavior[20] and the absence of bound magnetic polarons[24] seen in Fe-based DMS's.

Co-based DMS's have also been recently studied,[29–37] and the first successful growth of true alloys of such a material, $Zn_{1-x}Co_xSe$, was achieved by molecular-beam epitaxy, yielding single-crystal epilayers on GaAs(001) substrate.[29,30] The Co^{2+} in ZnSe has a level splitting which is intermediate in complexity between its Mn- and Fe-doped counterparts: the $^4F_{9/2}$ free-ion ground level of Co^{2+} ($3d^7$) is split by the tetrahedral crystal field into an upper $^4T_1$ orbital triplet, a $^4T_2$ triplet, and a lower $^4A_2$ orbital singlet ground state.[38] Unlike Mn^{2+}, the Co^{2+} ground state has a significant orbital angular momentum component due to spin-orbit mixing with the low-lying $^4T_2$ triplet, producing a larger effective Landé g factor (2.27 in Co vs. 2.00 Mn).[39,40]

Many optical studies of these systems have been focused on the effects of *sp-d* interaction on the fundamental band-gap energy at the Γ point of the Brillouin zone (BZ).[4,17,41–43] However, to our knowledge, no systematic study has yet been reported about the optical response of Zn(Mn,Fe,Co)Se at higher photon energies. For device applications, knowledge of the optical response over a wide energy is of great importance. Because higher interband transitions usually occur in different places within the Brillouin zone with different symmetry, studies of higher band-gap energies can also produce new results which are not obtainable at the Γ point. In this paper, we present dielectric-function spectra of single crystal $Zn_{1-x}A_xSe$ (A=Mn,Fe,Co) ($0 \le x < 0.14$) films between 3.5 and 5.5 eV using spectroscopic ellipsometry measurements. In particular we study the composition-dependent interband transitions E_1 and $E_1+\Delta_1$ at the L point.

Automatic spectroscopic ellipsometry is an excellent

technique for investigating the optical response of semiconductors[44] and has been used to study Si,[45,46] Ge,[45,47] as well as III-V (Refs. 45 and 48–55) and II-VI (Refs. 56–62) compound semiconductors and their alloys. An accurate determination of the energy threshold (E), linewidth (Γ), and phase (ϕ) of the critical points is obtained through the analysis of numerical second derivative spectra of the complex dielectric constant with respect to the photon energy, $d^2\epsilon/dw^2$. In our study, we find that the linewidths increase with x for all alloys, while the energies decrease with x for $Zn_{1-x}Mn_xSe$ and increase with x for $Zn_{1-x}Fe_xSe$ and $Zn_{1-x}Co_xSe$. The *sp-d* exchange interaction model[42] is calculated to second order in perturbation theory at the L point to try to explain the $Zn_{1-x}Mn_xSe$ system. However, the work done by Kim, Chang and Klein[63] has demonstrated that the effects of *sp-d* hybridization[17,58,64] need to be considered to fully explain the behavior in all the systems.

Section II describes the sample preparation and the experimental technique. In Sec. III the dielectric functions of $Zn_{1-x}(Mn,Fe,Co)_x$ Se are presented. Section IV assesses the influence of the *s-d* and *p-d* exchange interactions on the dependence of the band gaps of $Zn_{1-x}(Mn,Fe,Co)_xSe$ on x, and finally the *sp-d* hybridization effect is introduced.

II. EXPERIMENT

The $Zn_{1-x}(Mn,Fe,Co)_xSe$ layers were grown by molecular-beam epitaxy on GaAs(001) substrates. All the samples show the zinc-blende crystal structure and are paramagnetic. The thickness of the layers ranged from 0.2 to 2 μm. The maximum alloy compositions (x) included in this study were 0.144, 0.122, and 0.094 for $Zn_{1-x}Mn_xSe$, $Zn_{1-x}Fe_xSe$, and $Zn_{1-x}Co_xSe$, respectively. Details about the growth conditions and the characterizations are found in Refs. 25–27 and 29–31.

Dielectric function spectra $\epsilon(\omega)=\epsilon_1(\omega)+i\epsilon_2(\omega)$ were measured at room temperature between 3.5 and 5.0 eV using an automatic spectroscopic rotating analyzer ellipsometer of the type developed by Aspnes.[65,66] After being dispersed by a Cary 14R monochromator, the light from a 75-W xenon lamp is linearly polarized with a Rochon-quartz prism. Upon reflection from the sample the linear-polarized light becomes elliptically polarized. The reflected light is modulated by means of a rotating analyzer (Rochon prism) and detected by a photomultiplier. The output of the photomultiplier is digitized and the signal is analyzed with the aid of a personal computer. The measurements were generally performed at an incident angle of 68.4°.

The sample was mounted and optically aligned with an He-Ne laser in a windowless cell in flowing purified N_2 to minimize surface contamination. It is well known that the existence of overlayers on the surface complicates efforts to obtain the intrinsic dielectric response of the sample using ellipsometry.[45] Therefore, the samples have to be etched *in situ* immediately before the measurement. We followed the wet chemical etching procedure described in Ref. 62, where the successful removal of the oxide overlayer on ZnSe was reported. The chemical treatment was repeated until real-time ellipsometric spectra showed no more changes and the highest values of ϵ_2 at the $E_1+\Delta_1$ band-gap energy region were obtained. Figure 1 shows the imaginary part of the pseudodielectric function after chemical treatment of one of the samples ($Zn_{0.947}Mn_{0.053}Se$). The pseudodielectric function $\langle\epsilon\rangle$ is defined as the measured or apparent dielectric function obtained by reducing the ellipsometric data with the two-phase (ambient-substrate) model,[67] ignoring the presence of possible surface overlayers and microscopic roughness. Each spectrum represents the final spectrum taken after various stages of our chemical etching procedure, starting with the bottom spectrum to the top. The spectra have been offset. The change in the spectrum after each chemical treatment is similar to that found for ZnSe.[62] The results of the methanol and acetone treatment were a simple decrease of the dielectric constant below the E_1 band gap and an increase above the band gap, demonstrating that overlayers were being successfully removed. Upon using a 1:3 mixture of NH_4OH (29%):methanol, the E_1 peak shifted to higher energy and $E_1+\Delta_1$ peak was significantly enhanced. To determine whether we removed the natural oxide overlayer using the above chemical etching procedure, Auger electron spectroscopy (AES) experiment was used to examine the surface. The disappearance of an oxygen peak after our chemical etching procedure demonstrated that the 1:3 mixture of NH_4OH (29%):methanol removed the oxide overlayer on these samples.

III. RESULTS

The real and imaginary parts of the pseudodielectric function $\langle\epsilon\rangle$ for $Zn_{1-x}Mn_xSe$ in the 3.5–5.5 eV range are shown in Fig. 2. The spectra have been offset as indicated. The structures corresponding to the E_1 and $E_1+\Delta_1$ transitions shift slightly to lower energies and broaden to merge into a single peak as the Mn content in-

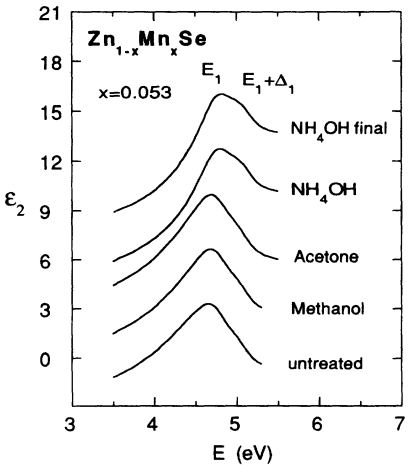

FIG. 1. Imaginary part of the pseudodielectric function $\langle\epsilon\rangle$ of the $Zn_{0.947}Mn_{0.053}Se$ film (5859 Å) with consecutive chemical etchings described as in Ref. 62. Spectra are shifted by units of 3 to the central spectrum of acetone treatment.

creases. Extra structures below 4 eV in the 2.2% and 14.4% samples arise from interference effects due to the small thickness of the thin film. However, even though all the spectra we report in this paper are measured from the films, since the films thicknesses are substantially larger than the critical thickness for strain relaxation, those measured are expected to reflect the dielectric response of the bulk. Several studies of the effects of strain in ZnSe films grown on GaAs (Refs. 68–70) confirm that most of our thin films are in the "bulk" region, and we do not see a shift of the energy gap expected for strain even in relatively thin samples.

To perform a line-shape analysis of the structures in our spectra, and thus to obtain values of the CP parameters, the second derivatives of the dielectric spectra were numerically calculated.[71] An appropriate level of smoothing was also allowed in order to suppress the noise in the derivative spectra without distorting the line shape. Due to the small size of the samples and the reduced intensity of our light source for photon energies above the $E_1+\Delta_1$ band gap, we found that the best compromise between the signal-to-noise ratio and resolution was obtained by using the second derivative. The resulting spectra were fitted to the standard analytic critical point (interband transition) line shape:[72,73]

$$\frac{d^2\epsilon}{d\omega^2}=\begin{cases} n(n-1)Ae^{i\phi}(\omega-E+i\Gamma)^{n-2}, & n\neq 0 \\ Ae^{i\phi}(\omega-E+i\Gamma)^{-2}, & n=0 \end{cases} \quad (1)$$

where a critical point is described by the amplitude A, threshold energy E, broadening Γ, and excitonic phase angle ϕ. The exponent n has the values $-\frac{1}{2}$, 0, and $\frac{1}{2}$ for one-, two-, (logarithmic), and three-dimensional critical points, respectively. Discrete excitons are represented by $n=-1$. For the excitonic line shape, a phase angle $\phi\neq 0$ corresponds to a line shape resulting from the interaction of a discrete excitation with a continuous background.[50] A least-square procedure was used for the fit, with both the real and the imaginary parts of $d^2\epsilon/d\omega^2$ fitted simultaneously. We found that the derivatives of the dielectric function associated with all the CP peaks could be best fit with excitonic line shapes, as was reported in Refs. 46, 61, and 62. All spectra of E_1 and $E_1+\Delta_1$ were fit simultaneously with the same phase angle ϕ for both CP's.[47,50,51] For fits with $\Gamma(E_1)$ and $\Gamma(E_1+\Delta_1)$ as free parameters, we found $\Gamma(E_1+\Delta_1)$ to be larger than $\Gamma(E_1)$ at low composition x, but smaller for larger x values. Similar behavior was also observed in $Al_{1-x}Ga_xAs$ (Ref. 53) and in the temperature dependence of InP.[51] This was interpreted as an artifact of the fit occurring when Γ is comparable to the energy separation between E_1 and $E_1+\Delta_1$ and was fit the same values for both CP's.[51] The E_1 and $E_1+\Delta_1$ band-gap energies obtained with and without these constraints differ by less than the experimental errors.[62] We find that the constrained CP parameters (e.g., ϕ_1 and ϕ_2) are the average of the two values obtained when not constrained. Another approach to investigating the CP's is to make a Fourier analysis of the raw spectrum as suggested by Aspnes.[74] This method gives very precise CP parameters without using numerical derivative procedures. It may be desirable to use this method for our spectra, and we plan to address this in future work.

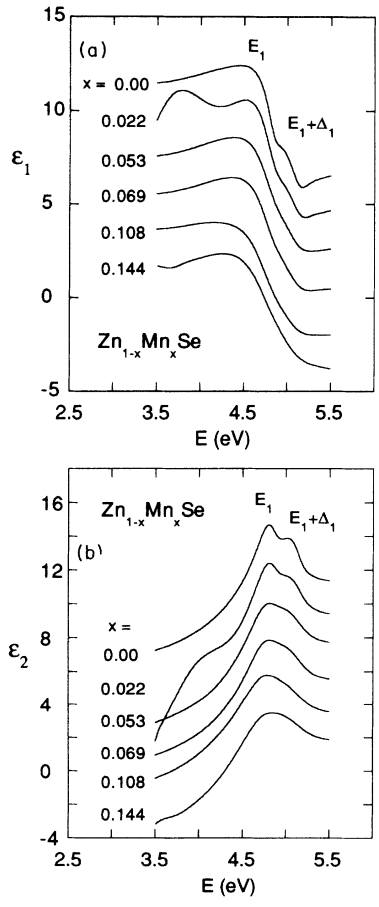

FIG. 2. (a) Real part and (b) imaginary part of the pseudodielectric function $\langle\epsilon\rangle=\langle\epsilon_1\rangle+i\langle\epsilon_2\rangle$ of $Zn_{1-x}Mn_xSe$ for several compositions. Spectra have been offset by increments of 2 relative to the center spectrum of the 5.3% sample.

In Fig. 3 we display the second-derivative spectra of $Zn_{1-x}Mn_xSe$ together with the best fits using Eq. (1). The dots represent experimental data for $d^2\epsilon_1/d\omega^2$ (those for $d^2\epsilon_2/d\omega^2$ are not shown for clarity, but the quality of the fits is similar). In the Mn 14.4% sample, while it is hard to resolve two peaks in the raw spectra (Fig. 2), the derivative spectrum in Fig. 3 clearly shows the existence of two peaks, and a redshift of the E_1 peak is easily seen. In Figs. 4 and 5, we represent the pseudodielectric functions of $Zn_{1-x}Fe_xSe$ and $Zn_{1-x}Co_xSe$. Again, the thinner films show the interference patterns up to 4 eV in $Zn_{1-x}Fe_xSe$. However, the interference patterns in $Zn_{1-x}Co_xSe$ diminish below 3.0 eV, because these films are thicker than 1.0 μm. Therefore the small structure near 4.3 eV at high compositions in $Zn_{1-x}Co_xSe$ is an intrinsic feature and is not due to interference effects. The identification of this peak will be discussed elsewhere.[75] In all alloys the E_1 and $E_1+\Delta_1$ transitions broaden to merge into a single peak as x increases.

Figure 6 shows the composition dependence of the line

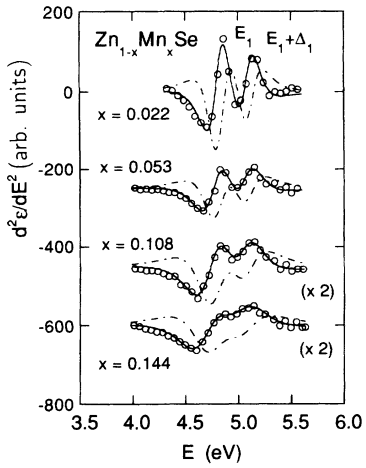

FIG. 3. Fits to the second derivatives of the real (solid) and imaginary (dashed) parts of the dielectric function of $Zn_{1-x}Mn_xSe$. The dots represent experimental data for $d^2\epsilon_1/d\omega^2$. To show the quality of the fits clearly, we reduced the number of data point in the graph to one-third.

broadenings for all three alloys fitted by Eq. (1) with the same values for both E_1 and $E_1+\Delta_1$ transitions as mentioned before. The increase in the linewidths with alloying is undoubtedly due to fluctuations in the alloy composition caused by the random distribution of Zn and magnetic ions at cation sites.[76] Values for the same phase angle obtained for both E_1 and $E_1+\Delta_1$ transitions are shown in Fig. 7. A phase angle ϕ has been used in the literature[57,58,77,78] as a phenomenological measure of excitonic effects on the line shapes. The dependence of ϕ on x shown in Fig. 7 is reasonable if ϕ is a measure of excitonic effects: they should become smaller with increasing disorder and thus reach a minimum for $x \cong 0.5$. Similar behavior has been found in $Cd_{1-x}Hg_xTe$ (Ref. 57) and $Cd_{1-x}Mn_xTe$.[58] The fitted amplitudes are more or less composition independent (Fig. 8). The ratio $A(E_1)/A(E_1+\Delta_1)$ is on average 1.3–1.4.

IV. DISCUSSION AND ANALYSIS

Figure 9 illustrates the fitted E_1 and $E_1+\Delta_1$ transition energies for all three $Zn_{1-x}(Mn,Fe,Co)_xSe$ alloys as a function of x, obtained from Eq. (1). In $Zn_{1-x}Mn_xSe$, both E_1 and $E_1+\Delta_1$ transition energies decrease with in-

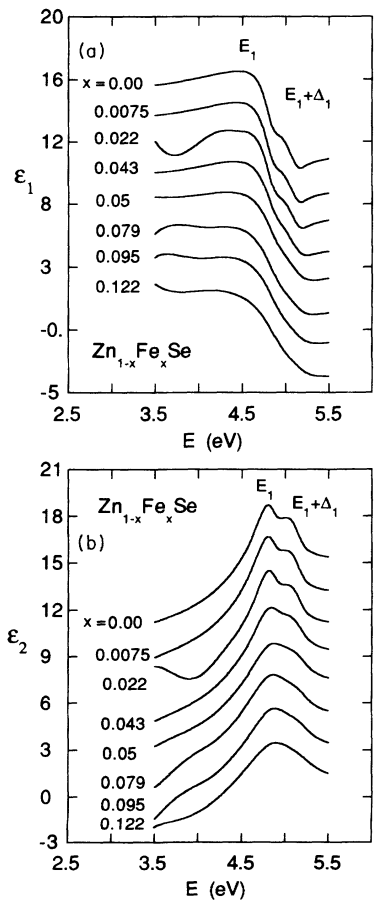

FIG. 4. (a) Real part and (b) imaginary part of the pseudodielectric function $\langle\epsilon\rangle=\langle\epsilon_1\rangle+i\langle\epsilon_2\rangle$ of $Zn_{1-x}Fe_xSe$ for several compositions. Spectra have been offset by increments of 2 relative to the center spectrum of the 5.0% sample.

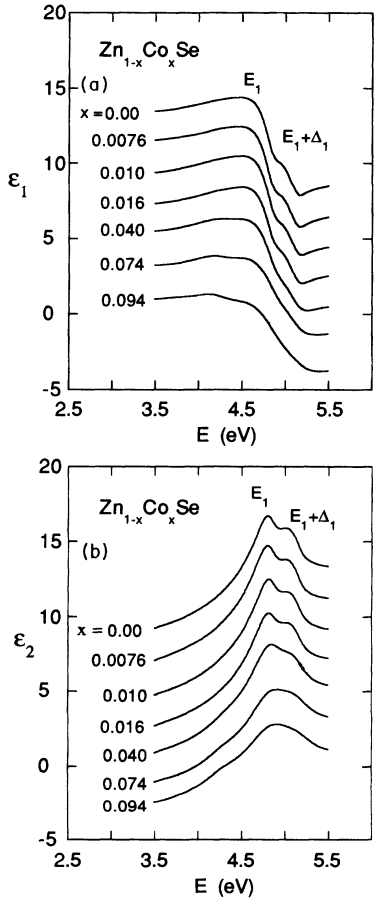

FIG. 5. (a) Real part and (b) imaginary part of the pseudodielectric function $\langle\epsilon\rangle=\langle\epsilon_1\rangle+i\langle\epsilon_2\rangle$ of $Zn_{1-x}Co_xSe$ for several compositions. Spectra have been offset by 2 to each other from the center spectrum of 1.6% sample.

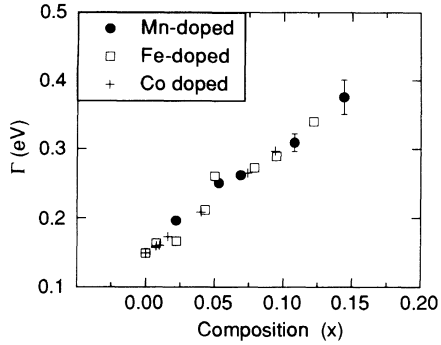

FIG. 6. Dependence of the linewidth on composition x defined in Eq. (1) for $Zn_{1-x}Mn_xSe$ (filled circles), $Zn_{1-x}Fe_xSe$ (open rectangles), and $Zn_{1-x}Co_xSe$ (crosses).

creasing x, while in $Zn_{1-x}Fe_xSe$ and $Zn_{1-x}Co_xSe$, the E_1 and $E_1+\Delta_1$ energies increase with x. These results are striking in that the band gaps of $Zn_{1-x}Mn_xSe$ are expected to increase with x since the fundamental E_0 band gap of MnSe is reportedly larger than that of ZnSe.[79]

An unusual initial decrease of the fundamental band-gap energy E_0 has been reported in $Zn_{1-x}Mn_xSe$ (Refs. 4 and 80) and $Cd_{1-x}Mn_xS$,[80,81] while other Mn alloys such as $Zn_{1-x}Mn_xTe$,[82] $Cd_{1-x}Mn_xTe$,[82-84] $Cd_{1-x}Mn_xSe$,[82,85,86] and $Hg_{1-x}Mn_xTe$ (Ref. 87) show the linearly varying band-gap energies. Recently, the decrease of E_0 in $Zn_{1-x}Mn_xSe$ was reported up to $x\sim0.15$ at room temperature.[88] This initial decrease cannot be explained on the basis of a broadening and shifting of energy levels due to statistical fluctuations of the crystal potential in an alloy (band-gap bowing). To explain the composition dependence of E_0 in $Zn_{1-x}Mn_xSe$, a model[89-91] describing the effects of the *sp-d* exchange interaction between the Mn *d* electrons and the band electrons was applied.[42] The authors of Ref. 42 found that this contribution successfully explains the initial decrease of E_0 band gap with increasing x, showing that for low x there is a correlation between the measured magnetic susceptibility and the deviation of E_0 from a linear dependence on x. In order to understand this unusual dependence of the L point band-gap energies on x, we have examined the possible influence of the *sp-d* exchange interaction on the E_1 and $E_1+\Delta_1$ band-gap energies.

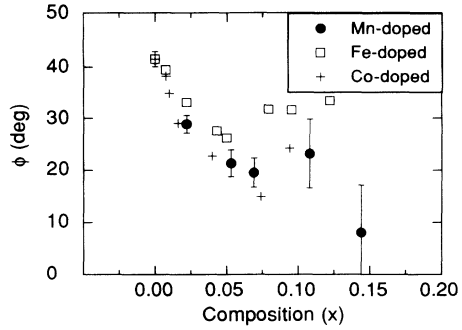

FIG. 7. Dependence on composition x of the excitonic parameters defined in Eq. (1) for $Zn_{1-x}Mn_xSe$ (filled circles), $Zn_{1-x}Fe_xSe$ (open rectangles), and $Zn_{1-x}Co_xSe$ (crosses).

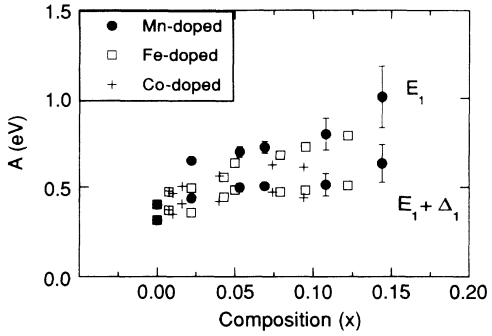

FIG. 8. Dependence on composition x of the amplitude parameters defined in Eq. (1) for E_1 and $E_1+\Delta_1$ critical points for $Zn_{1-x}Mn_xSe$ (filled circles), $Zn_{1-x}Fe_xSe$ (open rectangles), and $Zn_{1-x}Co_xSe$ (crosses).

A. *sp-d* exchange interaction model

Figure 10 shows the band structure of ZnSe calculated by Ren, Kim, and Chang,[92] using a nonlocal empirical pseudopotential method. Several interband transitions related to CP's at different parts of the BZ are indicated. It is easily seen that the conduction and valence bands are spherically symmetric at the Γ point, but at the L point they are asymmetric and saddle pointlike, respectively. When the Λ_6^c and $\Lambda_{4,5}^v$ (Λ_6^v) energy bands are nearly parallel, the E_1 ($E_1+\Delta_1$) critical point has contributions not only from the L point but also from the Λ bands.[93-95] In ZnSe, however, the Λ bands are nearly parallel only in the region close to the L point (Fig. 10), so in the following we consider only the L point contribution to simplify the calculation.

1. *Band shifts due to exchange interaction*

The commonly used *sp-d* exchange Hamiltonian for describing the coupling of band electrons and localized

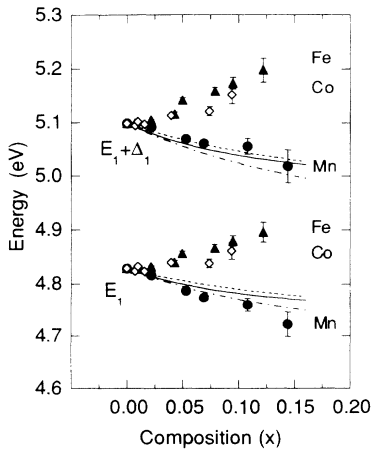

FIG. 9. Composition dependence of E_1 and $E_1+\Delta_1$ energies of $Zn_{1-x}Mn_xSe$ (filled circles), $Zn_{1-x}Fe_xSe$ (filled triangles), and $Zn_{1-x}Co_xSe$ (open diamonds). Lines represent the estimated values from the Eq. (11) using $D=0.1$ eV and $q_0=6.6\times10^7$ cm^{-1} for $Zn_{1-x}Mn_xSe$ (dot-dashed), $Zn_{1-x}Fe_xSe$ (dotted), and $Zn_{1-x}Co_xSe$ (solid).

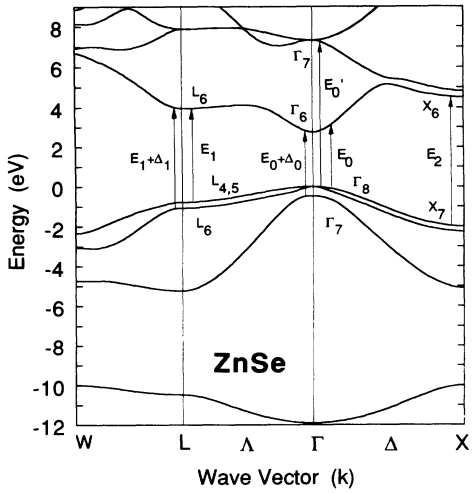

FIG. 10. Electronic energy band structure of ZnSe [Ren, Kim, and Chang (Ref. 92)].

magnetic impurity spins is given as[96,97]

$$H=\sum_n J(\mathbf{r}-\mathbf{R}_n)\mathbf{s}\cdot\mathbf{S}_n \ , \tag{2}$$

where $J(\mathbf{r}-\mathbf{R}_n)$ is the exchange integral for an electron with spin $\mathbf{s}$ at $\mathbf{r}$ and a magnetic ion with spin $\mathbf{S}_n$ at $\mathbf{R}_n$. The unperturbed wave functions at the L point for the conduction and valence bands are given by

$$\begin{aligned} |k\sigma\rangle_c &= \frac{1}{\sqrt{V}} e^{i\mathbf{k}\cdot\mathbf{r}}\phi_c(\mathbf{r})\chi_\sigma^c \ , \\ |k\sigma\rangle_v &= \frac{1}{\sqrt{V}} e^{i\mathbf{k}\cdot\mathbf{r}}\phi_v(\mathbf{r})\chi_\sigma^v \ , \end{aligned} \tag{3}$$

respectively, where V is the volume of the crystal, ϕ is the simple periodic Bloch amplitude, and χ denotes the spin part of the wave functions. The angular and spin parts are chosen as in Refs. 93 and 98,

$$\begin{aligned} \phi_c&: \ (A|S\rangle+B|\bar{z}\rangle)|\uparrow,\downarrow\rangle \ ; \\ \phi_v&: \ \left|\frac{1}{\sqrt{2}}(\bar{X}+i\bar{Y})\uparrow\right\rangle , \ \left|\frac{1}{\sqrt{2}}(\bar{X}-i\bar{Y})\downarrow\right\rangle , \\ &\quad \left|\frac{1}{\sqrt{2}}(\bar{X}+i\bar{Y})\downarrow\right\rangle , \ \left|\frac{1}{\sqrt{2}}(\bar{X}-i\bar{Y})\uparrow\right\rangle , \end{aligned} \tag{4}$$

where the upper bar denotes the projection of the wave function at the Γ point along the [111] direction and upper and lower parts in the valence-band wave function apply to $L_{4,5}^v$ and L_6^v bands, respectively (Fig. 10). The unperturbed energy for the conduction band at the L point is approximated as an asymmetric minimum, $E_k^c=E_0^c-\hbar^2k_t^2/2m_t^c-\hbar^2k_l^2/2m_l^c$. For the valence bands, $E_k^v=E_0^v-\hbar^2k_t^2/2m_t^v+\hbar^2k_l^2/2m_l^v$ applies to both the $L_{4,5}^v$ and L_6^v bands with different effective masses, where m_t and m_l are the transverse and longitudinal effective masses. The longitudinal direction is chosen along the [111] direction.

The first-order perturbation given by Eq. (2) is proportional to $\langle S^z\rangle$, which is the thermal average of S^z. All our $Zn_{1-x}(Mn,Fe,Co)_xSe$ samples show paramagnetic behavior at room temperature. Therefore in the absence of an external magnetic field $\langle S^z\rangle$ is equal to zero and has no contribution to the energy gap to first order.

The second-order perturbation correction to the conduction band is given by

$$E_c^{(2)}=-\tfrac{1}{2}\frac{m_t^c q_0}{\pi^2\hbar^2}\left[\frac{\alpha\Omega_0}{2}\right]^2\frac{k_BT}{(g\mu_B)^2}(\chi^z+2\chi_\perp)x_c \times\ln\left[\frac{1+x_c}{1-x_c}\right] , \tag{5}$$

where $x_c=\sqrt{(m_l^c-m_t^c)/m_l^c}$, Ω_0 is the elementary unit cell volume,[43] and α is defined by

$$\Omega_0\alpha(\mathbf{k}-\mathbf{k}')=\int d^3r\, e^{i(\mathbf{k}-\mathbf{k}')\cdot\mathbf{r}}J(r)|\phi_c(r)|^2 \ . \tag{6}$$

We approximate $\alpha(q)$ by[42]

$$\alpha(q)=\begin{cases}\alpha \ , & q\le q_0 \\ 0 \ , & q>q_0 \ .\end{cases} \tag{7}$$

In Eq. (5) $\chi^z=\chi^{zz}$ and $\chi_\perp=\chi^{xx}=\chi^{yy}$ are the magnetic susceptibilities which can be taken from an independent experiment, and in Eq. (7) q_0 is the cutoff wave vector, i.e., we assume $\alpha(q)$ to be a step function due to the short-ranged nature of $J(r)$.[42] Since all the parameters in Eq. (5) are positive, the correction pulls the conduction band at the L point down to lower energies.

For the $L_{4,5}^v$ valence band, the result is given by

$$E_{v4,5}^{(2)}=\frac{q_0}{\pi^2\hbar^2}\left[\frac{\beta\Omega_0}{2}\right]^2\frac{k_BT}{(g\mu_B)^2} \times[\chi^zM(E_1)+2\chi_\perp M(E_1+\Delta_1)] , \tag{8}$$

where the exchange parameter β has the same definition as α in Eqs. (6) and (7), but involves valence band states, $M(E_1)$ is a function of effective masses for the $L_{4,5}^v$ valence band, and $M(E_1+\Delta_1)$ is that for the L_6^v valence band, where, for instance,

$$M(E_1)=\frac{m_t^{E_1}}{2}x_0\ln\left[\frac{1+x_0}{1-x_0}\right] ,$$

with

$$x_0=\left[\frac{m_l^{E_1}}{m_t^{E_1}+m_l^{E_1}}\right]^{1/2} .$$

The second-order energy correction for the L_6^v valence band is

$$E_{v6}^{(2)}=\frac{q_0}{\pi^2\hbar^2}\left[\frac{\beta\Omega_0}{2}\right]^2\frac{k_BT}{(g\mu_B)^2} \times[\chi^zM(E_1+\Delta_1)+2\chi_\perp M(E_1)] . \tag{9}$$

Therefore, a rigid shift of the valence band also occurs, however, with opposite sign to that of the conduction band.

2. Shifts of L point transition energies

Since all the materials of our study are essentially cubic, we have $\chi^z=\chi_\perp=\chi$. The resultant energy correction for E_1 is

$$\Delta E_1^{(2)}=-\frac{q_0}{\pi^2\hbar^2}\left[\frac{\Omega_0}{2}\right]^2\frac{k_BT}{(g\mu_B)^2}\chi[M_\alpha\alpha^2+M_\beta\beta^2]\,, \tag{10}$$

where M_α and M_β represent the mass contributions defined in Eqs. (5) and (8), respectively. The spin-split part $\Delta(E_1+\Delta_1)^{(2)}$ has same formula but a different value of M_β. Since all the values in Eq. (10) are positive, the overall effect of the second-order perturbation correction to the transition energies is negative, which means that the E_1 and $E_1+\Delta_1$ transition energies should be reduced by the correction of exchange interaction effects. Therefore this result predicts that there should be a decrease of band-gap energies with increasing magnetic ion concentrations if this second-order magnetic interaction is larger than the correction due to lattice effects.

3. Estimation of parameters

To estimate the magnitude of this magnetic energy correction we need to obtain values for the parameters in Eq. (10). High-temperature magnetic susceptibility values for $Zn_{1-x}(Mn,Fe,Co)_xSe$ (Refs. 99, 22, and 32, respectively) are available as a function of temperature and concentration and were fit to the Curie-Weiss law. Figure 11(a) shows χ from this fit at room temperature as a function of composition. The values of α and β, which are the interaction parameters between the magnetic impurities and the conduction- and valence-band electrons, respectively [see Eq. (6)], have not been studied at the L point. However, those at the Γ point have been reported (see Table I). The α values are similar for all three alloys. The variation in β is much larger with Co having the largest β value and Mn the smallest. Since the wave functions at the L point are linear combinations of those at the Γ point [Eq. (4)], the exchange integral values α and β at the L point can be described by the same linear combinations as those at the Γ point. Tight-binding calculations[100] have been carried out to determine these coefficients in Eq. (4). For the conduction band, a mixing of s-like and p-like states occurs at the L point, and thus α at the L point is a mixture of α and β at the Γ point ($\alpha_L=0.37\alpha_\Gamma+0.114\beta_\Gamma$). However, for the valence band, β values are taken to be the same as those at the Γ point ($\beta_L=\beta_\Gamma$). There is some variation in the reported values of α and β, and therefore we have chosen the average of the entries in Table I for each material. Since there are no reported values of the effective masses at the L point of ZnSe, we have estimated those from the band structure shown in Fig. 10. Final estimates of $\Delta E_1^{(2)}$ in Eq. (10) are shown in Fig. 11(b) in units of eV/q_0. The result of the calculation for $\Delta(E_1+\Delta_1)^{(2)}$ is not shown, but is similar, since there is no significant difference between the value of $M(E_1+\Delta_1)$ and $M(E_1)$ in Eqs. (8) and (9). Clearly the magnitude of the magnetic interaction energy correction

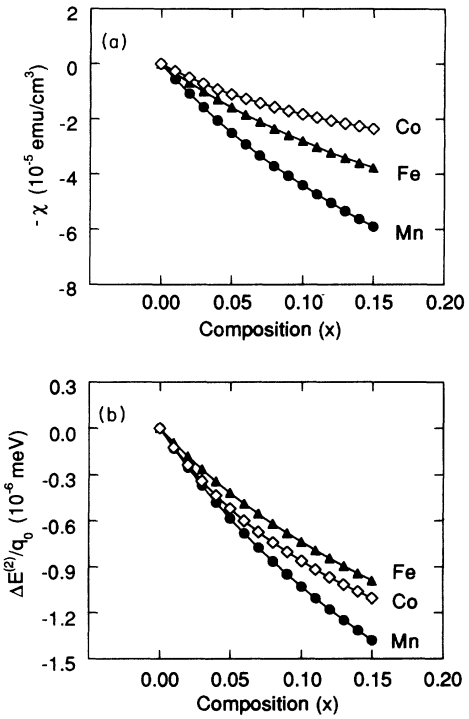

FIG. 11. Composition dependence of (a) reported magnetic susceptibilities χ and (b) the calculated magnetic interaction energy $\Delta E_1^{(2)}$ (in the unit of eV/q_0) of $Zn_{1-x}Mn_xSe$ (filled circles), $Zn_{1-x}Fe_xSe$ (filled triangles), and $Zn_{1-x}Co_xSe$ (open diamonds).

in $Zn_{1-x}Mn_xSe$ is much larger than those in $Zn_{1-x}Fe_xSe$ and $Zn_{1-x}Co_xSe$. Together, this result illustrates that, although the magnetic susceptibility of $Zn_{1-x}Co_xSe$ is smaller than that of $Zn_{1-x}Fe_xSe$, its β value is much larger, leading to a larger second-order perturbation energy in $Zn_{1-x}Co_xSe$ than in $Zn_{1-x}Fe_xSe$.

4. Comparison with experimental data

The total estimated E_1 band-gap energy equation used for comparison with the data in Fig. 9 is given by

$$E_1(x)=E_1^0+Dx+\Delta E_1^{(2)}(x)\,, \tag{11}$$

where the parameter D is the energy shift due to lattice parameter changes with alloying. Since the D value at

TABLE I. Reported α and β values at the Γ point for $Zn_{1-x}(Mn,Fe,Co)_xSe$.

	α (eV)	β (eV)	Reference
$Zn_{1-x}Mn_xSe$	0.29	−1.4	4
	0.26	−1.31	5
	0.26	−1.11	79
$Zn_{1-x}Fe_xSe$	0.22	−1.57	20
	0.226	−1.334	23
$Zn_{1-x}Co_xSe$	0.231	−2.179	34[a]
	0.231	−1.853	37

[a]We used α value from Ref. 37 to get the β value in Ref. 34, which reports the (α-β) value.

the L point has not been studied, we assume that the D value at the L point is about half that at the Γ point, as is the case for most zinc-blende semiconductor ternaries,[101-105] and we find $D=0.1$ eV for $Zn_{1-x}Mn_xSe$.[79] Using this D value, we adjust the cutoff wave vector q_0 to get a reasonable fit to the $Zn_{1-x}Mn_xSe$ data with Eq. (11). The best-fit curve is shown in Fig. 9, corresponding to a q_0 value of 6.6×10^7 cm^{-1}, which is 0.6 of the distance to the BZ boundary. This value is a little bit too large to be consistent with our perturbation model around the L point in k space even though it is not far from those reported from the temperature-dependent energy gap studies at the Γ point in $Zn_{1-x}Mn_xSe$ ($q_0=3.3\times10^7$ cm^{-1})[42], $Cd_{1-x}Mn_xTe$ ($q_0=6.6\times10^7$ cm^{-1}),[106] and $Cd_{1-x}Mn_xSe$ ($q_0=3.8\times10^7$ cm^{-1}).[107] Additionally, this model cannot explain the $Zn_{1-x}Fe_xSe$ and $Zn_{1-x}Co_xSe$ cases at all. The D values for $Zn_{1-x}Fe_xSe$ and $Zn_{1-x}Co_xSe$ might be different from that of $Zn_{1-x}Mn_xSe$, but not a factor of 10 larger, which is necessary to explain our data. Therefore we conclude that while the *sp-d* exchange interaction model seems to explain $Zn_{1-x}Mn_xSe$ band-gap energies at the L point, it fails to predict those of $Zn_{1-x}Fe_xSe$ and $Zn_{1-x}Co_xSe$.

Adding lattice bowing effect to our model [in Eq. (11)] would make the result worse since this contribution should have an effect on the band gap which is similar to the *sp-d* interaction. Further, the estimated band-gap energy shift to lower energy by the disorder-induced bowing effect (the Vechter-Berolo-Woolley model[108]) is only 4 meV at $x=0.1$ in this material, which would have no significant effect on the result. The assumption that the spin-spin interaction model of Eq. (2) applies to all three kinds of magnetic impurities is not unreasonable. For example, although Fe^{2+} and Co^{2+} ions have nonzero orbital angular momentum in their ground state, which differs from that in Mn^{2+}, the orbital angular momenta of Fe^{2+} and Co^{2+} are quenched in the crystal field environment. Therefore, this spin-only exchange Hamiltonian of Eq. (2) should be sufficient to account for the exchange interactions in $Zn_{1-x}Fe_xSe$ and $Zn_{1-x}Co_xSe$. Our calculation also assumes that the isotropic magnetic susceptibility χ is q independent since the neutron-scattering spectrum shows that the q-dependent peak disappears at room temperature.[109] More detailed calculation of the exchange integral parameters of α and β, which includes fluctuations in the local concentration of the magnetic ions and q dependence,[43] and other types of magnetic interaction such as superexchange may improve the analysis of this data. However, the failure of the *sp-d* exchange interaction model to explain the differences between Mn-, Fe-, and Co-doped ZnSe is believed to occur because this model does not include any information on the relative position of the d levels in the band structure of the host material, ZnSe.

B. *sp-d* hybridization model

The effect of the *sp-d* hybridization on the band-gap energies was proposed in an ellipsometric study of the composition-dependent band-gap energies of $Cd_{1-x}Mn_xTe$ (Ref. 58) and has been analyzed in several theoretical studies on the same material.[17,64,110,111] In this hybridization model, the effect of *sp-d* exchange interaction is considered to be negligible. The effect of this hybridization on the E_1 band gap can be easily understood from Fig. 12, which shows the location of the magnetic impurity d levels in the ZnSe band structure of Fig. 10. The locations of d levels, which are not sensitive to the host materials,[16] are from Ref. 19, where the host material is CdSe. Since all three spin-up d levels are located below the valence band, the repelling effect of the *sp-d* hybridization will push the $L_{4,5}$ and L_6 valence bands upward for all three dopants. On the conduction band, Mn spin-down d levels will push the L_6 conduction band downward, whereas the Fe and Co d levels will push it upward, suggesting that this picture may explain the different behaviors observed for the three dopants in our data.

For quantitative analysis, the effect of this *sp-d* hybridization on the L-point band-gap energies has been calculated within a sp^3s^* empirical tight-binding model, and the detailed procedure will be published elsewhere.[63] To describe this system, the multisite Anderson Hamiltonian[15,16,111,112] is written as

$$H=\sum_{k,\mu}\epsilon_k n_{k\mu}+\left[\sum_{\mu}E_d n_{d\mu}+U n_{d\uparrow}n_{d\downarrow}\right]+\sum_{k,\mu}(V_{kd}C^{+}_{k\mu}C_{d\mu}+\text{H.c.})\,, \tag{12}$$

where μ denotes the electron spin states. The first term describes the pure ZnSe sp^3s^* bands determined by a tight-binding calculation which includes the alloying effect given by Dx in Eq. (11). The s^* orbital is added to adequately describe the conduction band. The second term represents five degenerate magnetic impurity d levels with electron-electron interactions of the Hubbard form. The relatively small splitting between e_g and t_{2g} levels in the tetrahedral crystal field is neglected for simplification. The last term corresponds to a hybridiza-

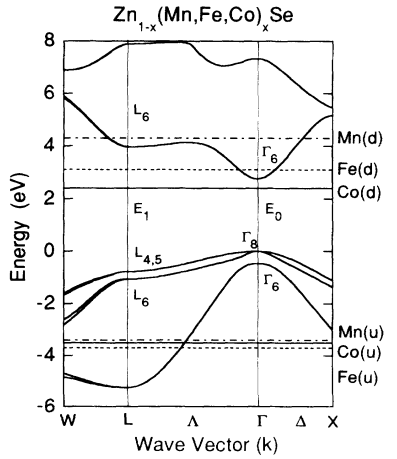

FIG. 12. The positions of the d-band levels from Ref. 19 are shown in ZnSe band structure of Fig. 10. The positions of Mn (dot-dashed), Fe (dotted), and Co (solid) d levels are shown as horizontal lines. The (u) and (d) denote the conventionally defined spin-up and spin-down $3d$ levels as in Refs. 58 and 111.

tion between band electrons and d electrons which yields a shift of the band energies and a broadening of the d levels. In the calculation, the hybridization potential of the atomic orbital $V_{pd\sigma}$ is the only adjustable parameter needed to reproduce the reported Γ point band-gap energy splitting (i.e., α and β) under applied magnetic field, because the other two atomic hybridization potentials $V_{pd\pi}$ and V_{sd} were assumed to follow Harrison's ratio.[113] Using the E_d and U values from Ref. 19, the values obtained for $V_{pd\sigma}$ are -1.267, -1.148, and -1.083 eV for Mn-, Fe-, and Co-doped ZnSe, respectively. With these hybridization parameters and $D=0.2$ eV, shifts of the L point band-gap energies are estimated and shown in Fig. 13. Remarkably, this model quantitatively explains the increase of band gaps in $Zn_{1-x}Fe_xSe$ and $Zn_{1-x}Co_xSe$.

We note that the exchange integral β defined in Eqs. (6) and (8) has been interpreted as the p-d exchange interaction (potential exchange[96,97]) and has been widely used to explain the magnetic and optical properties of several DMS systems.[42,89–91] More recently β has been interpreted as the p-d hybridization interaction (kinetic exchange).[15–19] In our analysis, the interaction mechanism between the band electrons and the impurity d electrons is considered to be a pure direct sp-d exchange interaction in the exchange interaction model (Sec. IV A) and a pure sp-d hybridization term in the hybridization model (Sec. IV B). The hybridization model appears to reasonably describe our data, suggesting that the hybridization interaction between sp and d electron is the dominant interaction in this system. However, as is pointed out in Ref. 19, since there are considerable uncertainties in the interpretation of the photoemission data, in particular the position of the d levels and the values of U (or U_{eff}), this quantitative agreement between our analysis and the data should be viewed with caution. We also find that since both the p-d and the s-d hybridization effects in our model are zero at the conduction-band minimum at the Γ point, the hybridization model alone cannot explain the α value.[15,16] Therefore, more work needs to be done to study the interplay between the hybridization and the exchange interaction contribution, and further systematic experiments on the E_1 and $E_1+\Delta_1$ band gaps will be needed (particularly the temperature and magnetic-field dependences).

V. CONCLUSIONS

We have measured the dielectric function of ZnSe and $Zn_{1-x}(Mn,Fe,Co)_xSe$ alloy films grown on GaAs(001) substrates by means of spectroscopic ellipsometry in the 3.5–5.5 eV region. A chemical etching procedure to remove the natural oxide overlayer was developed to obtain the pure dielectric response of these alloys. Significant improvement of the ellipsometric signal was achieved by a solution of 1:3 mixture of NH_4OH (29%):methanol, and the successful removal of oxide layers was confirmed by Auger studies. By performing a line-shape analysis of the structures observed, the CP parameters for E_1 and $E_1+\Delta_1$ were obtained. With the utility of the chemical etching procedure the separation of the two peaks could be detected up to $x=14.4\%$ of $Zn_{1-x}(Mn,Fe,Co)_xSe$. An initial decrease of the E_1 and $E_1+\Delta_1$ peaks of $Zn_{1-x}Mn_xSe$ with x is observed. We calculated the effect of the sp-d exchange interaction on the L point band-gap energies to find that this effect can explain only the $Zn_{1-x}Mn_xSe$ case marginally. On the other hand, the sp-d hybridization model[63] explains all $Zn_{1-x}(Mn,Fe,Co)_xSe$ systems quite satisfactorily. Therefore we attribute this doping dependence to the effect of the sp-d hybridization effect on the L point band-gap energies. To confirm this hybridization effect, additional systematic studies such as temperature- and magnetic-field-dependent experiments should be done.

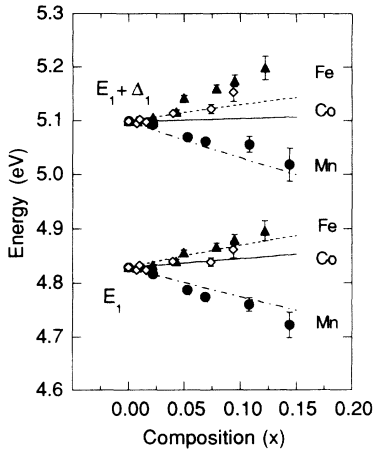

FIG. 13. Estimated composition-dependent band gap energies from the Eq. (12) using $D=0.2$ eV are shown as lines for $Zn_{1-x}Mn_xSe$ (dot-dashed), $Zn_{1-x}Fe_xSe$ (dotted), and $Zn_{1-x}Co_xSe$ (solid). Dots represent the data of Fig. 9.

ACKNOWLEDGMENTS

Y.D.K. wishes to thank Y. C. Chang for valuable discussions. AES experiments were carried out in the Center for Microanalysis of Materials, University of Illinois, which is supported by DOE under Contract No. DEFG02-91ER45439. Y.D.K. and M.V.K. were supported by NSF Grant No. DMR 89-20538 and S.L.C. by DOE Grant. No. DEFG02-91ER45439. The work at NRL was supported by the office of Naval Research.

[1] N. B. Brandt and V. V. Moshchkalov, Adv. Phys. **33**, 193 (1984).

[2] J. K. Furdyna and J. Kossut, in *Semiconductors and Semimetals*, edited by R. K. Willardson and A. C. Beer (Academic, San Diego, 1988), Vol. 25.

[3] Y. G. Semenov and B. D. Shanina, Phys. Status Solidi. B **104**, 631 (1981).

[4] A. Twardowski, T. Dietl, and M. Demianiuk, Solid State Commun. **48**, 845 (1983).

[5] A. Twardowski, M. V. Ortenberg, M. Demianiuk, and R. Pau-

thenet, Solid State Commun. **51**, 849 (1984).
[6]J. Mycielski, Proc. Cryst. Growth Char. **10**, 101 (1985).
[7]D. Coquillat, J. P. Lascaray, M. C. Deruelle, J. A. Gaj, and R. Triboulet, Solid State Commun. **59**, 25 (1986).
[8]J. K. Furdyna and N. Samarth, J. Appl. Phys. **61**, 3526 (1987).
[9]K. C. Hass and H. Ehrenreich, J. Cryst. Growth **86**, 8 (1988).
[10]X. Liu, A. Petrou, J. Warnock, B. T. Jonker, G. A. Prinz, and J. J. Krebs, Phys. Rev. Lett. **63**, 2280 (1989).
[11]B. T. Jonker, X. Liu, W. C. Chou, A. Petrou, J. Warnock, J. J. Krebs, and G. A. Prinz, J. Appl. Phys. **69**, 6097 (1991).
[12]W. C. Chou, A. Petrou, J. Warnock, and B. T. Jonker, Phys. Rev. Lett. **67**, 3820 (1991).
[13]N. Dai, H. Luo, F. C. Zhang, N. Samarth, M. Dobrowolska, and J. K. Furdyna, Phys. Rev. Lett. **67**, 3824 (1991).
[14]B. T. Jonker, W. C. Chou, A. Petrou, and J. Warnock, J. Vac. Sci. Technol. A **10**, 1458 (1992).
[15]A. K. Bhattacharjee, G. Fishman, and B. Coqblin, Physica B **117&118**, 449 (1983).
[16]B. E. Larson, K. C. Hass, H. Ehrenreich, and A. E. Carlsson, Phys. Rev. B **37**, 4137 (1988).
[17]P. M. Hui, H. Ehrenreich, and K. C. Hass, Phys. Rev. B **40**, 12 346 (1989).
[18]J. Masek, Solid State Commun. **78**, 351 (1991).
[19]A. K. Bhattacharjee, Phys. Rev. B **46**, 5266 (1992).
[20]A. Twardowski, P. Glod, W. J. M. de Jonge, and M. Demianiuk, Solid State Commun. **64**, 63 (1987).
[21]F. S. Pool, J. Kossut, U. Debska, and R. Reifenberger, Phys. Rev. B **35**, 3900 (1987).
[22]A. Twardowski, A. Lewicki, M. Arciszewska, W. J. M. de Jonge, H. J. M. Swagten, and M. Demianiuk, Phys. Rev. B **38**, 10 749 (1988).
[23]X. Liu, A. Patrou, B. T. Jonker, G. A. Prinz, J. J. Krebs, and J. Warnock, Appl. Phys. Lett. **53**, 46 (1988).
[24]D. Heiman, A. Petrou, E. D. Isaacs, S. H. Bloom, Y. Shapira, and W. Giriat, Phys. Rev. Lett. **60**, 1876 (1988).
[25]B. T. Jonker, S. B. Qadri, J. J. Krebs, and G. A. Prinz, Appl. Phys. Lett. **50**, 848 (1987).
[26]B. T. Jonker, J. J. Krebs, S. B. Qadri, G. A. Prinz, F. Volkening, and N. C. Koon, J. Appl. Phys. **63**, 3303 (1988).
[27]B. T. Jonker, S. B. Qadri, J. J. Krebs, and G. A. Prinz, J. Vac. Sci. Technol. A **6**, 1946 (1988).
[28]W. Low and M. Weger, Phys. Rev. **118**, 1119 (1960).
[29]B. T. Jonker, J. J. Krebs, and G. A. Prinz, Appl. Phys. Lett. **53**, 450 (1988).
[30]B. T. Jonker, S. B. Qadri, J. J. Krebs, G. A. Prinz, and L. Salamanca-Young, J. Vac. Sci. Technol. A **7**, 1360 (1989).
[31]B. T. Jonker, J. J. Krebs, G. A. Prinz, X. Liu, A. Petrou, and L. Salamanca-Young, in *Growth, Characterization and Properties of Ultrathin Magnetic Films and Multilayers,* edited by B. T. Jonker, J. P. Heremans, and E. E Marinero, MRS Symposia Proceedings No. 151 (Materials Research Society, Pittsburgh, 1989), p. 151.
[32]A. Lewicki, A. I. Schindler, J. K. Furdyna, and W. Giriat, Phys. Rev. B **40**, 2379 (1989).
[33]J. J. Krebs, B. T. Jonker, and G. A. Prinz, IEEE Trans. Magn. **24**, 2548 (1988).
[34]X. Liu, A. Petrou, B. T. Jonker, J. J. Krebs, G. A. Prinz, and J. Warnock, J. Appl. Phys. **67**, 4796 (1990).
[35]C. J. Chen, W. Gao, Z. F. Qin, W. Hu, M. Qu, and W. Giriat, J. Appl. Phys. **70**, 6277 (1991).
[36]H. J. M. Swagten, A. Twardowski, P. J. T. Eggenkamp, and W. J. M. de Jonge, Phys. Rev. B **46**, 188 (1992).
[37]J. P. Lascaray, F. Hamdani, D. Coquillat, and A. K. Bhattacharjee, J. Magn. Magn. Mater. **104-107**, 995 (1992).
[38]A. Abragam and B. Bleaney, *Electron Paramagnetic Resonance of the Transition Ions* (Oxford University Press, London, 1970), p. 470.
[39]F. S. Ham, G. W. Ludwig, G. D. Watkins, and H. H. Woodbury, Phys. Rev. Lett. **5**, 468 (1960).
[40]U. Kaufman and J. Schneider, Solid State Commun. **25**, 1113 (1978).
[41]K. J. Ma and W. Giriat, Solid State Commun. **60**, 927 (1986).
[42]R. B. Bylsma, W. M. Becker, J. Kossut, and U. Debska, Phys. Rev. B **33**, 8207 (1986).
[43]S. M. Ryabchenko, Y. G. Semenov, and O. V. Terletskii, Phys. Status Solidi B **144**, 661 (1987).
[44]D. E. Aspnes, in *Optical Properties of Solids: New Developments,* edited by B. O. Seraphin (North-Holland, Amsterdam, 1976), p. 799.
[45]D. E. Aspnes and A. A. Studna, Phys. Rev. B **27**, 985 (1983).
[46]P. Lautenschlager, M. Garriga, L. Viña, and M. Cardona, Phys. Rev. B **36**, 4821 (1987).
[47]L. Viña, S. Logothetidis, and M. Cardona, Phys. Rev. B **30**, 1979 (1984).
[48]S. M. Kelso, D. E. Aspnes, M. A. Pollack, and R. E. Nahory, Phys. Rev. B **26**, 6669 (1982).
[49]D. E. Aspnes, S. M. Kelso, R. A. Logan, and R. Bhat, J. Appl. Phys. **60**, 754 (1986).
[50]P. Lautenschlager, M. Garriga, S. Logothetidis, and M. Cardona, Phys. Rev. B **35**, 9174 (1987).
[51]P. Lautenschlager, M. Garriga, and M. Cardona, Phys. Rev. B **36**, 4813 (1987).
[52]S. Zollner, C. Lin, E. Schönherr, A. Böhringer, and M. Cardona, J. Appl. Phys. **66**, 383 (1989).
[53]S. Logothetidis, M. Cardona, and M. Garriga, Phys. Rev. B **43**, 11 950 (1991).
[54]H. Yao, P. G. Snyder, and J. A. Woolam, J. Appl. Phys. **70**, 3261 (1991).
[55]A. R. Heyd, R. W. Collins, K. Vedam, S. S. Bose, and D. L. Miller, Appl. Phys. Lett. **60**, 2776 (1992).
[56]H. Arwin and D. E. Aspnes, J. Vac. Sci. Technol. A **2**, 1316 (1984).
[57]L. Viña, C. Umbach, M. Cardona, and L. Vodopyanov, Phys. Rev. B **29**, 6752 (1984).
[58]P. Lautenschlager, S. Logothetidis, L. Viña, and M. Cardona, Phys. Rev. B **32**, 3811 (1985).
[59]S. Logothetidis, M. Cardona, P. Lautenschlager, and M. Garriga, Phys. Rev. B **34**, 2458 (1986).
[60]K. Kumazaki, L. Viña, C. Umbach, and M. Cardona, Phys. Stat. Solidi B **156**, 371 (1989).
[61]S. Adachi and T. Taguchi, Phys. Rev. B **43**, 9569 (1991).
[62]Y. D. Kim, S. L. Cooper, M. V. Klein, and B. T. Jonker, Appl. Phys. Lett. **62**, 2387 (1993).
[63]Y. D. Kim, Y. C. Chang, and M. V. Klein, Phys. Rev. B **48**, 17 770 (1993).
[64]K. C. Hass, in *Semimagnetic Semiconductors and Diluted Magnetic Semiconductors,* edited by M. Averous and M. Balkanski (Plenum, New York, 1991), p. 59.
[65]D. E. Aspnes, Opt. Commun. **8**, 222 (1973).
[66]D. E. Aspnes and A. A. Studna, Appl. Opt. **14**, 220 (1975).
[67]R. M. A. Azzam and N. M. Bashara, *Ellipsometry and Polarized Light* (North-Holland, Amsterdam, 1977).
[68]J. E. Potts, H. Cheng, S. Mohapatra, and T. L. Smith, J. Appl. Phys. **61**, 333 (1987).
[69]K. Ohkawa, T. Mitsuyu, and O. Yamazaki, Phys. Rev. B **38**, 12 465 (1988).
[70]W. Bala, M. Drozdowski, and M. Kozielski, Phys. Status Solidi A **130**, K195 (1992).

[71]A. Savitzky and J. E. Gollay, Anal. Chem. **36**, 1627 (1974).
[72]M. Cardona, *Modulation Spectroscopy,* Suppl. 11 of *Solid State Physics,* edited by F. Seitz, D. Turnbull, and H. Ehrenreich (Academic, New York, 1969).
[73]D. E. Aspnes, in *Handbook on Semiconductors,* edited by M. Balkanski (North-Holland, Amsterdam, 1980), Vol. 2, p. 109.
[74]D. E. Aspnes, Surf. Sci. **135**, 284 (1983).
[75]Y. D. Kim, S. L. Cooper, M. V. Klein, J. H. Park, J. W. Allen, and B. T. Jonker (unpublished).
[76]E. F. Schubert, E. O. Gobel, Y. Horikoshi, K. Ploog, and H. J. Queisser, Phys. Rev. B **30**, 813 (1984).
[77]J. E. Rowe and D. E. Aspnes, Phys. Rev. Lett. **25**, 162 (1970).
[78]L. Viña and M. Cardona, Phys. Rev. B **29**, 6739 (1984).
[79]J. K. Furdyna, J. Appl. Phys. **64**, R29 (1988).
[80]K. J. Ma and W. Giriat, Phys. Status Solidi A **95**, K135 (1986).
[81]M. Ikeda, K. Itoh, and H. Sato, J. Phys. Soc. Jpn. **25**, 455 (1968).
[82]Y. R. Lee, A. K. Ramdas, and R. L. Aggarwal, Phys. Rev. B **38**, 10 600 (1988).
[83]M. P. Vecchi, W. Giriat, and L. Videla, Appl. Phys. Lett. **38**, 99 (1981).
[84]N. Bottka, J. Stankiewicz, and W. Giriat, J. Appl. Phys. **52**, 4189 (1981).
[85]W. Giriat and J. Stankiewicz, Phys. Status Solidi A **59**, K79 (1980).
[86]J. Stankiewicz, Phys. Rev. B **27**, 3631 (1983).
[87]J. K. Furdyna, J. Vac. Sci. Technol. **21**, 220 (1982).
[88]C. D. Poweleit, L. M. Smith, S. L. Cooper, and B. T. Jonker, Bull. Am. Phys. Soc. **37**, 292 (1992).
[89]F. Rys, J. S. Helman, and W. Baltensperger, Phys. Kondens. Mater. **6**, 105 (1967).
[90]C. Hass, Phys. Rev. **168**, 531 (1968).
[91]J. Diouri, J. P. Lascaray, and M. E. Amrani, Phys. Rev. B **31**, 7795 (1985).
[92]S. F. Ren, Y. D. Kim, and Y. C. Chang (unpublished).
[93]F. H. Pollak and M. Cardona, Phys. Rev. **172**, 816 (1968).
[94]S. Koeppen, P. Handler, and S. Jasperson, Phys. Rev. Lett. **27**, 265 (1971).
[95]D. E. Aspnes and J. E. Rowe, Phys. Rev. B **7**, 887 (1972).
[96]J. Kossut, Phys. Status Solidi B **78**, 537 (1976).
[97]G. Bastard, C. Rigaux, and A. Mycielski, Phys. Status Solidi B **79**, 585 (1977).
[98]M. Cardona, in *Light Scattering in Solids II,* edited by M. Cardona and G. Güntherodt (Springer-Verlag, Berlin, 1982), p. 119.
[99]J. K. Furdyna, N. Samarth, R. B. Frankel, and J. Spalek, Phys. Rev. B **37**, 3707 (1988).
[100]Y. D. Kim and Y. C. Chang (unpublished).
[101]A. G. Thompson, M. Cardona, K. L. Shaklee, and J. C. Woolley, Phys. Rev. **146**, 601 (1966).
[102]E. W. Williams, Phys. Rev. **172**, 798 (1969).
[103]O. Berolo and J. C. Wooley, Can. J. Phys. **49**, 1335 (1971).
[104]K. Saito, A. Abina, and T. Takahashi, Solid State Commun. **11**, 841 (1972).
[105]S. Isomura, F. G. D. Prat, and J. C. Woolley, Phys. Status Solidi B **65**, 213 (1974).
[106]J. A. Gaj and A. Golnik, Acta Phys. Pol. A **71**, 197 (1987).
[107]L. Bryja and J. A. Gaj, Acta Phys. Pol. A **73**, 459 (1988).
[108]J. A. V. Vechten, O. Berolo, and J. C. Woolley, Phys. Rev. Lett. **29**, 1400 (1972).
[109]G. Dolling, T. M. Holden, V. F. Sears, J. K. Furdyna, and W. Giriat, J. Appl. Phys. **53**, 7644 (1982).
[110]S. Wei and A. Zunger, Phys. Rev. B **35**, 2340 (1987).
[111]K. C. Hass and H. Ehrenreich, Acta Phys. Pol. A **73**, 933 (1988).
[112]P. W. Anderson, Phys. Rev. **124**, 41 (1961).
[113]W. A. Harrison, *Electronic Structure and the Properties of Solids* (Dover, New York, 1989).